Modeling radiation characteristics of semitransparent media containing bubbles or particles

Jaona Randrianalisoa and Dominique Baillis

Centre de Thermique de Lyon–UMR CNRS 5008, Institut National des Sciences Appliquées de Lyon 69621, Villeurbanne Cedex, France

Laurent Pilon

Department of Mechanical and Aerospace Engineering, University of California, Los Angeles, 37-132 Engineering IV, Box 951597, Los Angeles, California 90095-1597

Received November 11, 2005; accepted December 27, 2005; posted February 7, 2006 (Doc. ID 65921)

Modeling of radiation characteristics of semitransparent media containing particles or bubbles in the independent scattering limit is examined. The existing radiative properties models of a single particle in an absorbing medium using the approaches based on (1) the classical Mie theory neglecting absorption by the matrix, (2) the far field approximation, and (3) the near field approximation are reviewed. Comparison between models and experimental measurements are carried out not only for the radiation characteristics but also for hemispherical transmittance and reflectance of porous fused quartz. Large differences are found among the three models predicting the bubble radiative properties when the matrix is strongly absorbing and/or the bubbles are optically large. However, these disagreements are masked by the matrix absorption during calculation of radiation characteristics of the participating medium. It is shown that all three approaches can be used for radiative transfer calculations in an absorbing matrix containing bubbles. © 2006 Optical Society of America

OCIS codes: 290.4020, 290.5850, 260.3060, 160.2750, 030.5620.

1. INTRODUCTION

Visible and infrared radiation transfer in semitransparent solids or liquids can be strongly affected by the presence of entrapped bubbles or particles. This is of interest in many practical engineering applications ranging from remote sensing of the ocean surface[1,2] to materials processing.[3,4]

Radiation transfer in particulate media has long been a subject of study, as reviewed by Viskanta and Mengüç[5] and Baillis and Sacadura.[6] Radiation characteristics of dispersed particles in a nonabsorbing medium have been extensively studied. The general way to obtain these radiation characteristics, based on the absorption and/or extinction and scattering efficiency factors and the scattering phase function, placed in a *nonabsorbing* environment, is by using the classical Mie theory (CMT).[7] However, few analyses have been carried out on the radiation characteristics of polydispersed bubbles in *absorbing* media. Fedorov and Viskanta[8] have proposed a model for the effective radiation characteristics of glass foams. Their analysis was performed for bubbles large compared with the wavelength of radiation in the limiting case of anomalous diffraction. Pilon and Viskanta[9] have studied the influence of the bubble size distributions and porosity by using the Fedorov and Viskanta model. Dombrovsky[10] questioned the validity of the previous models and suggested the use of the extended Mie theory[11] applied to the case of large gas bubbles in semitransparent liquid.

For estimating spurious scattering in optical elements, assessing the attenuation of light in fiber optics, and characterizing light transport through turbid water, a more rigorous prediction of light scattering and attenuation by spherical particles in absorbing media was developed.[11] Substituting into the CMT solutions the complex refraction index of the matrix instead of the real one is an inappropriate approximation. In fact, this neglects the attenuation of scattered waves by the absorbing matrix between the particle surface and the far field zone at which the CMT solutions were derived. In addition, the incident intensity needed to define the particle efficiency factors becomes questionable. The solutions should be derived from the solution of Maxwell's equations[7] over the particle surface. Two approaches are usually proposed: the far field approximation (FFA)[11–13] and the near field approximation (NFA).[14–19] The FFA was initially developed by Mundy *et al.*[11] and Chylek[12] by extending the CMT,[7] i.e., from a particle in a nonabsorbing environment to a particle in an absorbing environment. The FFA solutions such as the particle extinction[11] or absorption[12] and scattering efficiency factors were defined by using the true incident intensity on the particle instead of the conventional incident intensity at the particle center.[7] Sudiarta and Chylek[14,15] and Lebedev *et al.*[16,17] have proposed the NFA, in which the Poynting vectors (i.e., the solutions of Maxwell's equations[7]) are integrated over the particle surface.

Fu and Sun[18] used the NFA to model scattering and absorption efficiency factors of a coated particle placed in an absorbing medium. The scattering phase function derived from the FFA was used. Yang *et al.*[13] have extended the

FFA to study the scattering process and the polarization state during the interaction of an electromagnetic plane wave with a coated particle embedded in an absorbing environment. They analyzed the deviation between the extinction efficiency factor and the ratio of the scattering efficiency factor to the extinction efficiency factor from the NFA and FFA and discussed the application fields of these two approaches. They suggested that the FFA solutions, defined by using the conventional incident intensity at the particle center instead of the true incident intensity, should be used in order to preserve the usual meaning of radiation characteristics in the radiative transfer calculations. Recently, Sun *et al.*[19] compared the model of Fu and Sun[18] with a three-dimensional solution of Maxwell's equations,[7] using the numerical method known as finite-difference time domain,[20] for the radiative properties of a coated sphere placed in an absorbing matrix. Sharma and Jones[21] have studied the absorption and scattering of electromagnetic radiation by a large absorbing sphere containing highly absorbing inclusions. Their system (large sphere+particle inclusions) was approximated as a large sphere containing a homogeneous absorbing and scattering medium characterized by the radiation characteristics of the particle inclusions that use the NFA efficiency factors and the FFA scattering phase function. The ray tracing method, combined with the Monte Carlo technique, was used to determine the absorption and scattering of the incident radiation on the large homogeneous sphere.

Note that, to date, no model for the radiative properties of a particle (coated or uncoated) embedded in an absorbing medium is widely accepted. Therefore the aim of this study is (1) to clarify the issue concerning the appropriate definition of incident intensity to be applied for computing the efficiency factors of a single particle in an absorbing medium, (2) to determine the limits of application of the FFA, NFA, and CMT in the modeling of the radiation characteristics of an absorbing heterogeneous medium (in the CMT, the absorption of the matrix is taken into account in the effective absorption coefficient calculation but is neglected during the calculations of single particle radiative properties), and (3) to compare the radiation characteristics models based on the FFA, NFA, and CMT against the experimental data for porous fused quartz.[22]

In Section 2, models proposed to determine the radiation characteristics of an absorbing medium containing *polydispersed* bubbles from the single bubble radiative properties are first presented. Then, the existing models for predicting the radiative properties of a *single* particle or bubble in an absorbing medium are reviewed. The results obtained from the models are compared and discussed for different values of the complex index of refraction of the surrounding medium. Section 3 is concerned with porous fused quartz and a comparison of the experimental data with theoretical predictions.

2. THEORETICAL MODELS

A. Radiation Characteristics of a Semitransparent Medium Containing Polydispersed Bubbles

Let us consider spherical bubbles randomly distributed in a semitransparent matrix. We assume that there are no bubble clusters for a small concentration of bubbles, enabling one to treat the bubbles as independent scatterers.[23,24]

Thus the radiation characteristics such as the absorption coefficient α_λ and the scattering coefficients σ_λ of an absorbing continuous phase containing polydispersed spherical bubbles of radius a and size distribution $n(a)$ (Ref. 21) (or number of bubbles per unit volume having radius between a and $a+da$) such that $x=2\pi a/\lambda>1$ (Ref. 25) can be calculated as follows[9]:

$$\alpha_\lambda = \alpha_0 - \pi\int_0^\infty Q_m a^2 n(a)\mathrm{d}a = \alpha_0 - 0.75\frac{f_v}{a_{32}}\bar{Q}_m, \qquad (1)$$

$$\sigma_\lambda = \pi\int_0^\infty Q_s a^2 n(a)\mathrm{d}a = 0.75\frac{f_v}{a_{32}}\bar{Q}_s, \qquad (2)$$

where $\alpha_0=4\pi\kappa_0/\lambda$ is the absorption coefficient of the continuous phase, f_v is the bubble volume fraction or porosity, $\bar{Q}_s$ is the mean scattering efficiency factor for polydispersed bubbles, and $\bar{Q}_m$ is the mean absorption efficiency factor for polydispersed bubbles if they are filled with the matrix substance. The average radius a_{32} is defined as[10,25]

$$a_{32} = \frac{\int_0^\infty a^3 n(a)\mathrm{d}a}{\int_0^\infty a^2 n(a)\mathrm{d}a}. \qquad (3)$$

The mean efficiency factors $\bar{Q}_s$ and $\bar{Q}_m$ are expressed as[25]

$$\bar{Q}_j = \frac{\int_0^\infty Q_j a^2 n(a)\mathrm{d}a}{\int_0^\infty a^2 n(a)\mathrm{d}a} \quad \text{with } j=s \text{ or } m, \qquad (4)$$

where Q_s is the scattering efficiency factor of a bubble of radius a embedded in the host medium and Q_m is the absorption efficiency factor of a particle of radius a if it is filled with the matrix substance.[11,16,17] Q_m describes the ratio between the energy that would be absorbed by the matrix having size and shape equal to that of a bubble and the incident intensity on the bubble (which will be discussed in Subsection 2.B.4) multiplied by the bubble cross section πa^2. It has the same meaning as the absorption efficiency factor defined in the theory of light absorption and scattering by a particle.[7,23–27] The introduction of Q_m by means of $\bar{Q}_m$ in Eq. (1) indicates that the absorption coefficient of the porous medium is solely due to the matrix volume separating the bubbles.

Note that, in the case of monodispersed bubbles of radius a, a_{32} reduces to a and $\bar{Q}_s$ and $\bar{Q}_m$ are equal to Q_s and Q_m, respectively. In this case, summing Eqs. (1) and (2) yields the usual extinction coefficient of particles embedded in an absorbing matrix as defined by Lebedev *et al.*[16,17]

Moreover, the scattering phase function Φ_λ of the absorbing continuous phase containing polydispersed bubbles is given by the usual formulation for a nonabsorbing matrix[8–10,25]:

$$\Phi_\lambda(\Theta) = \frac{\pi}{\sigma_\lambda}\int_0^\infty Q_s\phi_\lambda(\Theta)a^2n(a)\mathrm{d}a = \frac{3f_v}{4\sigma_\lambda a_{32}}\frac{\int_0^\infty Q_s\phi_\lambda(\Theta)a^2n(a)\mathrm{d}a}{\int_0^\infty a^2n(a)\mathrm{d}a}, \quad (5)$$

where ϕ_λ is the scattering phase function of a single bubble of radius a and Θ is the angle between the incident and scattered radiations.

The asymmetry factor denoted by g, describing the relative ratio of the forward to backward scattering, is defined by[23–25]

$$g = \frac{1}{2}\int_0^\pi \Phi(\Theta)\cos\Theta\sin\Theta\mathrm{d}\Theta. \quad (6)$$

Note that, in practice, it is more useful to use (1) an approximated phase function such as the Henyey–Greenstein model[23,24] or (2) the transport approximations,[10,26] which depend essentially on the asymmetry factor.

B. Radiative Properties of a Single Particle in an Absorbing Medium

1. Classical Mie Theory

The Mie theory is the general way of determining the radiative properties such as the scattering (Q_s^M), absorption (Q_a^M), and extinction (Q_e^M) efficiency factors and the scattering phase function (ϕ^M) of a single particle in a nonabsorbing environment.[7,27] This theory was shown to be applicable for bubbles in semitransparent liquid[10] and will be used in this study for bubbles embedded in an absorbing matrix by ignoring the effect of the matrix absorption on Q_s^M, Q_a^M, Q_e^M, and ϕ^M.

Considering a bubble or particle with radius a illuminated by a monochromatic plane wave of wavelength λ in vacuum propagating in an attenuating and refracting medium with complex refraction index m_0, the independent parameters of the CMT solutions are the relative particle size parameter n_0x, where n_0 is the real part of the complex index m_0, and the relative complex refraction index of particle m/n_0, in which $m=n+j\kappa$ is the complex refraction index of the bubble or particle. The efficiency factors are given by[7,27]

$$Q_s^M(a) = \frac{2}{(n_0x)^2}\sum_{p=1}^\infty (2p+1)(|a_p|^2+|b_p|^2), \quad (7)$$

$$Q_e^M(a) = \frac{2}{(n_0x)^2}\mathrm{Re}\sum_{p=1}^\infty (2p+1)(a_p+b_p), \quad (8)$$

$$Q_a^M = Q_e^M - Q_s^M, \quad (9)$$

$$\phi^M(\Theta) = \frac{|S_1(\Theta)|^2+|S_2(\Theta)|^2}{\sum_{p=1}^\infty (2p+1)(|a_p|^2+|b_p|^2)}, \quad (10)$$

where a_p and b_p are the Mie coefficients expressed in terms of the Riccati–Bessel functions.[7,27] S_1 and S_2 are the usual amplitude functions,[7] and Re( ) corresponds to the real part of the complex number.

For an absorbing matrix, Q_m^M is required in Eq. (1). There is no established expression for Q_m^M in the conventional theory of scattering and absorption of radiation by a particle. However, Q_m^M can be derived from the expression for Q_a^M, since both have the same meaning. Indeed, Q_m^M can be computed from Eq. (9) by substituting the complex refraction index of the matrix for that of the bubble.

The asymmetry factor g^M related to the phase function ϕ^M is given by[7,23]

$$g^M = \frac{4\sum_{p=1}^\infty \{\mathrm{Re}[(p^2-1)(a_{p-1}a_p^*+b_{p-1}b_p^*)/p]+(2p-1)/(1-1/p)\mathrm{Re}(a_{p-1}b_{p-1}^*)\}}{(n_0x)^2Q_s^M}. \quad (11)$$

Here, the superscript * indicates the complex number conjugate.

For optically large bubbles (i.e., $x\gg1$) in an absorbing matrix, it can be shown that the CMT solutions for Q_m^M, Q_s^M, and g^M converge to the following asymptotic values:

$$Q_m^M = \frac{8\kappa_0x}{3} = \frac{4a_0}{3}, \quad (12)$$

$$Q_s^M = 2, \quad (13)$$

$$g^M = 1 - 0.45(n_0-1), \quad (14)$$

where $a_0=\alpha_0a$ is called the optical radius of a matrix particle.

Several studies[11–19] have highlighted the effects of the matrix absorption on the particle efficiency factors and the scattering phase function that were not accounted for in the CMT through Eqs. (7)–(14). The basic idea is to solve Maxwell's equations[7] by considering the complex refraction index of the matrix, m_0, and that of the particle, m. Two approaches are usually proposed to solve

Maxwell's equations: (1) the far field approximation (FFA)[10–13] and (2) the near field approximation (NFA).[14–19] These two approaches are detailed in Subsections 2.B.2 and 2.B.3.

2. Far Field Approximation

Mundy *et al.*[11] and Chylek[12] have suggested that the relations developed in the CMT based on the FFA, i.e., Eqs. (7)–(10), can be extended to analyze the radiative properties of a particle in an absorbing medium. For an arbitrary value of the complex refraction index of the surrounding medium, m_0, the classical Mie relations can be generalized by applying the FFA to the formulations of the scattered and extinction energy expressed in terms of the Poynting vector integral.[7,27] This extension consists in replacing, in the CMT solutions [Eqs. (7), (8), and (10)], (1) the relative particle size parameters n_0x by the complex value m_0x and (2) the complex particle refraction index m/n_0 by the corresponding relative value m/m_0. Thus the efficiency factors of a particle in an absorbing medium, such as Q_s^F and Q_e^F, can be obtained by multiplying the CMT solutions [i.e., Eqs. (7) and (8)] by a factor η such that

$$\eta = \frac{I_0}{I_i}\exp(-\alpha_0 r), \tag{15}$$

$$Q_s^F(r) = \frac{2\eta}{x^2|m_0|^2}\sum_{p=1}^{\infty}(2p+1)(|a_p|^2+|b_p|^2), \tag{16}$$

$$Q_e^F(r) = \frac{2\eta}{x^2|m_0|^2}\,\mathrm{Re}\sum_{p=1}^{\infty}(2p+1)(a_p+b_p), \tag{17}$$

where r is the radius of the integrating sphere in the far field zone ($r \gg a$) over which the integral of Poynting vectors is evaluated. The coefficients a_p and b_p are formally identical to those for a nonparticipating host medium except that the parameter n_0x is replaced by m_0x and m/n_0 by m/m_0. The incident intensity I_0 at the bubble center is evaluated in the absence of the bubble, while I_i is the incident intensity on the bubble. The latter will be discussed in Subsection 2.B.4.

The scattering phase function ϕ^F and the corresponding asymmetry factor g^F are similar to the CMT formulas given by Eqs. (10) and (11) but n_0x is replaced by m_0x and m/n_0 by m/m_0 in calculating the Mie coefficients a_p and b_p and the amplitude functions S_1 and S_2.

The efficiency factors $Q_s^F(r)$ and $Q_e^F(r)$ in Eqs. (16) and (17) are the scattering and extinction efficiency factors defined at distances far from the particle, i.e., in the far field zone, and depend not only on the matrix properties but also on the size r of the integrating sphere. In practice, the particle radiative properties should be independent of the integrating sphere. Usually, $Q_s^F(r)$ and $Q_e^F(r)$ are rescaled from the far field zone of radius r to the particle surface by applying a simple exponential factor $\exp[\alpha_0(r-a)]$ to Eqs. (16) and (17).[11,13] This makes the FFA efficiency factors $Q_s^F(a)$ and $Q_e^F(a)$ independent of the far field distance r, and they can be expressed as[11]

$$Q_s^F(a) = \frac{2\eta'}{x^2|m_0|^2}\sum_{p=1}^{\infty}(2p+1)(|a_p|^2+|b_p|^2), \tag{18}$$

$$Q_e^F(a) = \frac{2\eta'}{x^2|m_0|^2}\,\mathrm{Re}\sum_{p=1}^{\infty}(2p+1)(a_p+b_p), \tag{19}$$

with

$$\eta' = \frac{I_0}{I_i}\exp(-a_0). \tag{20}$$

Note that the extinction efficiency factor $Q_e^F(a)$ in Eq. (19) satisfies the relationship $Q_e^F(a)=Q_a^F(a)-Q_m^F(a)+Q_s^F(a)$.[11,18,19] This implies that $Q_e^F(a)$ does not have the same meaning as that of the conventional extinction efficiency factor for which $Q_e=Q_a+Q_s$. In addition, for a nonabsorbing bubble placed in an absorbing environment ($Q_a^F=0$), the absorption efficiency factor Q_m^F can be deduced from $Q_m^F=Q_s^F-Q_e^F$.[11]

3. Near Field Approximation

An alternative formulation known as the near field approximation (NFA) has been proposed by Sudiarta and Chylek,[14,15] Lebedev *et al.*,[16,17] Fu and Sun,[18] and Sun *et al.*[19] The energies absorbed and scattered by the particle are obtained by computing the integrals of the absorption and scattering Poynting vectors[7,27] over the scatterer surface as opposed to over the surface of a large imaginary sphere of radius r in the far field zone. This permits one to obtain the NFA efficiency factors such as Q_s^N, Q_a^N, and Q_m^N independently of the surrounding medium size as[14,15,18]

$$Q_s^N(a) = \frac{2I_0}{\mathrm{Re}\{\rho\}|\rho|^2 I_i}\,\mathrm{Re}\left\{\rho^*\sum_{p=1}^{\infty}(2p+1)i\left[-|a_p|^2\xi_p'(\rho)\xi_p^*(\rho) + |b_p|^2\xi_p(\rho)\xi_p'^*(\rho)\right]\right\}, \tag{21}$$

$$Q_a^N(a) = \frac{2I_0}{\mathrm{Re}\{\rho\}|\rho|^2 I_i}\,\mathrm{Re}\left\{\rho^*\sum_{p=1}^{\infty}(2p+1)i[-\psi_p'(\rho)\psi_p^*(\rho) - \psi_p(\rho)\psi_p'^*(\rho) + b_p\psi_p'^*(\rho)\xi_p(\rho) + b_p^*\psi_p(\rho)\xi_p'^*(\rho) - a_p\psi_p^*(\rho)\xi_p'(\rho) - a_p^*\psi_p'(\rho)\xi_p^*(\rho) + |a_p|^2\xi_p'(\rho)\xi_p^*(\rho) - |b_p|^2\xi_p(\rho)\xi_p'^*(\rho)]\right\}, \tag{22}$$

$$Q_m^N(a) = \frac{4I_0}{|\rho|^2 I_i}\sum_{p=1}^{\infty}(2p+1)\mathrm{Im}[\psi_p(\rho)\psi_p'^*(\rho)], \tag{23}$$

where $\psi(\rho)$, $\psi'(\rho)$, $\xi(\rho)$, and $\xi'(\rho)$ are the Ricatti–Bessel functions and their derivatives[28] with respect to the complex argument $\rho=m_0x$ while Im( ) refers to the imaginary part of the complex number. Note that here the extinction efficiency factor can be written as $Q_e^N=Q_s^N+Q_a^N$.[14,18]

In the literature, there is no established expression for the scattering phase function based on the NFA. Existing calculations[18,19,21] of absorption and scattering of electromagnetic radiation by particles using the NFA solutions

[Eqs. (21)–(23)] consider the same scattering phase function as that in the FFA. Similarly, in this work all calculations related to the NFA consider the FFA phase function.

Moreover, comparison between $Q_m^N(a)$ and $Q_m^F(a)$ tends to confirm that the absorption efficiency factors of a particle filled by the matrix substance from the FFA and NFA are identical, i.e., $Q_m^N(a)=Q_m^F(a)$. Indeed, the relative difference was found to be less than 0.5% for bubble size parameter x in the range from 1 to 10^{+4} in an absorbing matrix of optical index $n_0=1$ to 2 and $\kappa_0=0$ to 0.1. This is expected, since the absorption by the particle is independent of the observation zone at which the Poynting vectors are integrated.

4. Choice in the Definition of the Incident Intensity I_i

It is now necessary to discuss which expressions for the incident intensity I_i should be used in Eqs. (15)–(23) to define the efficiency factors of a bubble in an absorbing environment. Two definitions are commonly used: (1) I_i is equal to the intensity at the particle center, i.e., $I_i=I_0$,[13,16,17] and (2) I_i is equal to the average incident intensity on the particle, called the "truly incident intensity" and expressed as $I_i=\gamma I_0$.[11,12,14,15,18,19] The parameter γ is defined as the ratio of the incident energy over the particle illuminated area evaluated from the integral of the incident wave Poynting vector, to the incident energy

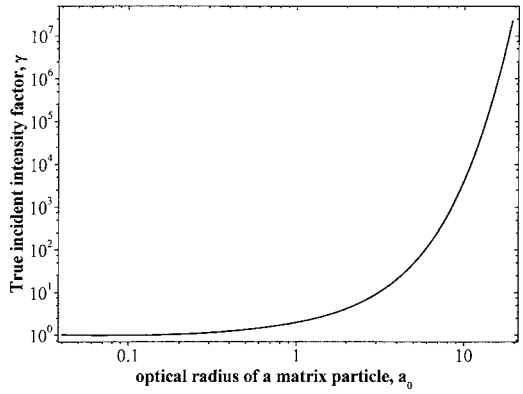

Fig. 1. Ratio between the intensities I_i and I_0 as a function of the optical radius of a matrix particle, a_0.

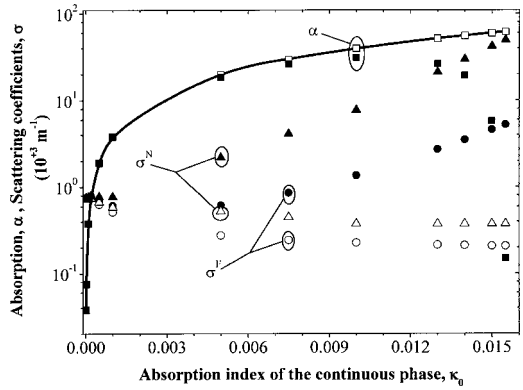

Fig. 2. Variation of the absorption (α) and scattering (σ) coefficients of a porous medium with $\lambda=\pi\,\mu$m, $x=200$, and $f_v=5\%$ as a function of κ_0: solid curve, α_0; open symbols, results from the definition $I_i=\gamma I_0$; solid symbols, results from the definition $I_i=I_0$.

over the particle of cross section πa^2 in the absence of the particle (i.e., the incident energy evaluated at the abscissa at the particle center). It is given by[11,13,14]

$$\gamma=\frac{1+(a_0-1)\exp(a_0)}{a_0^2}. \tag{24}$$

Figure 1 illustrates the variation of the parameter γ as a function of the parameter a_0. One can see that if $a_0<0.2$, then $\gamma\approx 1$ and the two definitions of intensity give identical results. Otherwise, one should be cautious in choosing the expression for the incident intensity I_i.

Let us analyze the variations in the effective absorption coefficient α [Eq. (1)] and scattering coefficient σ [Eq. (2)] of an absorbing medium containing monodispersed bubbles. The radiation wavelength at $\lambda=\pi\,\mu$m is considered. The bubble radius is taken equal to $a=100\,\mu$m, leading to a size parameter $x=200$ satisfying the criterion $x>1$. The bubble volume fraction f_v is taken equal to 5%, satisfying the independent scattering conditions for large particles.[29,30] The matrix refraction index n_0 can be chosen arbitrarily, since Q_m and Q_s become independent of n_0 for a large transparent bubble ($x\gg 1$ and $m=1$), as shown computationally in Subsection 2.B.5. The two definitions of intensities I_0 and γI_0 are used to determine Q_m and Q_s for both the NFA and FFA models. Figure 2 shows the variation of α and σ as functions of the matrix absorption κ_0. One can note that if the matrix absorption index κ_0 is increased and the incident intensity definition $I_i=\gamma I_0$ is used, the absorption coefficient of the porous medium, α, is (1) greater than the scattering coefficient σ for both the FFA and NFA and (2) of the same order of magnitude as that of the matrix absorption coefficient (α_0) due to the small void fraction. On the other hand, if the intensity definition $I_i=I_0$ is used, as suggested by Yang *et al.*,[13] then the scattering coefficient σ increases as κ_0 increases while the absorption coefficient α first increases with κ_0. Then, σ decreases slightly from $\kappa_0>0.005$ to finally decrease sharply to negative values from $\kappa_0>0.015$. On the contrary, this is not observed when the definition $I_i=\gamma I_0$ is used. Thus the definition $I_i=I_0$ seems to be inappropriate for computing the efficiency factors Q_e, Q_m, and Q_s of a bubble in an absorbing environment. Consequently, the definition of the incident intensity $I_i=\gamma I_0$ is used in the remainder of this study.

5. Comparison of Predictions of the Classical Mie Theory, Far Field Approximation, and Near Field Approximation

Comparison among CMT, FFA, and NFA calculations can be performed for the scattering efficiency factor and the scattering phase function or the asymmetry factor. Let us consider a bubble with $m=1$ embedded in matrices having different complex refraction indices $m_0=n_0+j\kappa_0$, such as $n_0=1.4$ and 1.7 and $\kappa_0=0.0$, 10^{-5}, 10^{-3}, 10^{-2}, and 0.1.

The scattering efficiency factors versus the particle size parameter are plotted in Fig. 3 for $n_0=1.4$ and in Fig. 4 for $n_0=1.7$. One can see that when $\kappa_0=0$, the absorption efficiency factor vanishes and the three approaches converge to the same solution. In the limiting case when $x\gg 1$, they converge to 2, which is the usual geometric optic limit for a nonabsorbing particle (bubble in this case).[23,27]

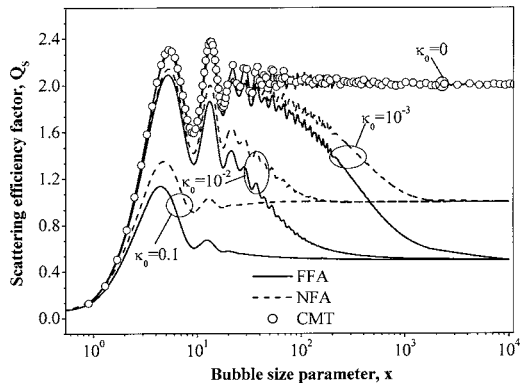

Fig. 3. Bubble scattering efficiency factor Q_s for $n_0=1.4$ as a function of the bubble size parameter x.

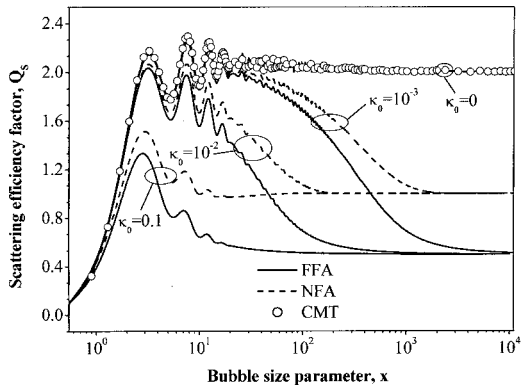

Fig. 4. Bubble scattering efficiency factor Q_s for $n_0=1.7$ as a function of the bubble size parameter x.

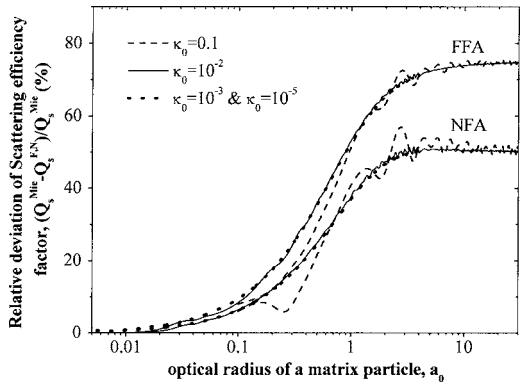

Fig. 5. Comparison among the FFA, NFA, and CMT scattering efficiency factors Q_s for $n_0=1.4$ versus optical radius of a matrix particle, a_0. Deviations for $\kappa_0=10^{-3}$ and $\kappa_0=10^{-5}$ are overlapping.

On the other hand, for an arbitrary value of $\kappa_0>0$, the FFA and NFA scattering efficiency factors converge asymptotically to 0.5 and 1, respectively. The FFA and NFA calculations give predictions similar to those of the CMT up to $a_0=0.06$ and 0.08, respectively, with relative deviation less than 5%, as illustrated in Figs. 5 and 6 as a function of the optical radius a_0. Figure 7 reports the relative deviation between the NFA and the FFA. Here, the relative deviation between the FFA and NFA predictions is less than 5% for $a_0<0.16$ and increases with a_0 to reach 90% for $a_0=20$.

The scattering phase functions from the FFA and NFA being equal, both approaches give the same asymmetry factor. Figures 8 and 9 compare the asymmetry factors g predicted by the FFA and the CMT for $n_0=1.4$ and 1.7, respectively. The figures show that the FFA and CMT remain in close agreement for $a_0<0.08$. Beyond this limit, the FFA is strongly influenced by the absorption by the surrounding medium, which is not taken into account in the CMT model.

Note that similar conclusions are reached when comparing the FFA, NFA, and CMT for the different matrix refraction indices (n_0). This tends to show that these con-

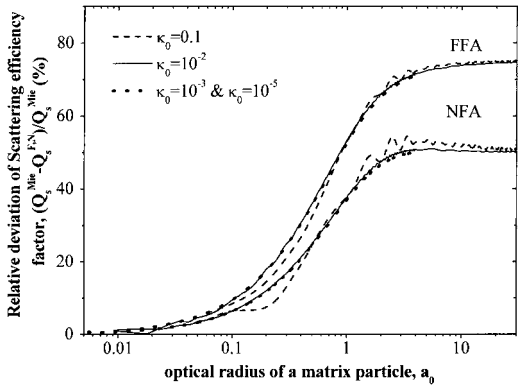

Fig. 6. Comparison among the FFA, NFA, and CMT scattering efficiency factors Q_s for $n_0=1.7$ versus optical radius of a matrix particle, a_0. Deviations for $\kappa_0=10^{-3}$ and $\kappa_0=10^{-5}$ are overlapping.

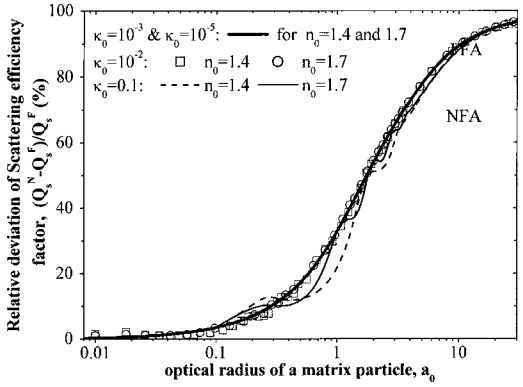

Fig. 7. Comparison among the FFA, NFA, and CMT scattering efficiency factors Q_s versus optical radius of a matrix particle, a_0. Deviations for $\kappa_0=10^{-3}$ and $\kappa_0=10^{-5}$ are overlapping.

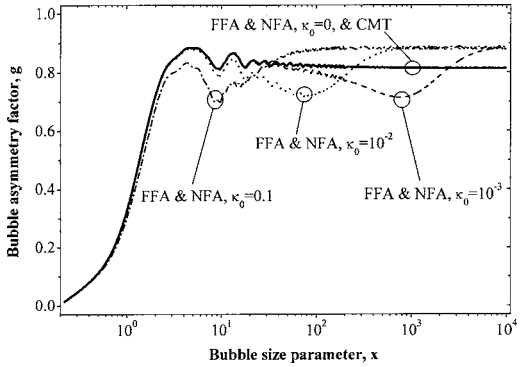

Fig. 8. Bubble asymmetry factor g for $n_0=1.4$. The predictions of g by the FFA and NFA are identical for the values of κ_0 considered. For $\kappa_0=0$, predictions by the FFA and NFA and the CMT are overlapping.

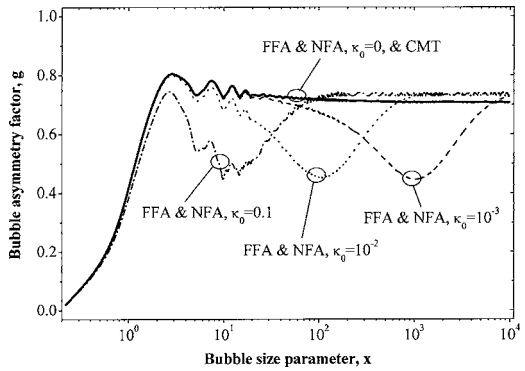

Fig. 9. Bubble asymmetry factor g for $n_0=1.7$. The predictions of g by the FFA and NFA are identical for the values of κ_0 considered. For $\kappa_0=0$, predictions by the FFA and NFA and the CMT are overlapping.

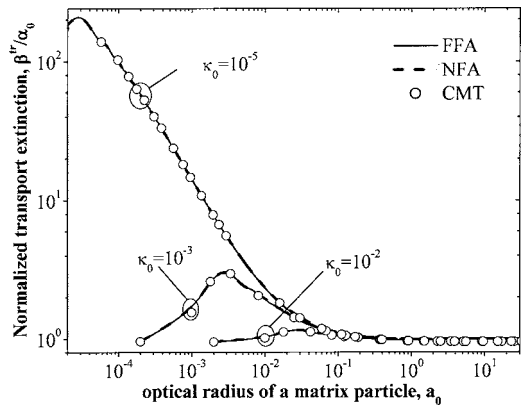

Fig. 10. Comparison among the CMT, NFA, and FFA transport extinctions β^{tr} for $n_0=1.4$ and $f_v=5\%$.

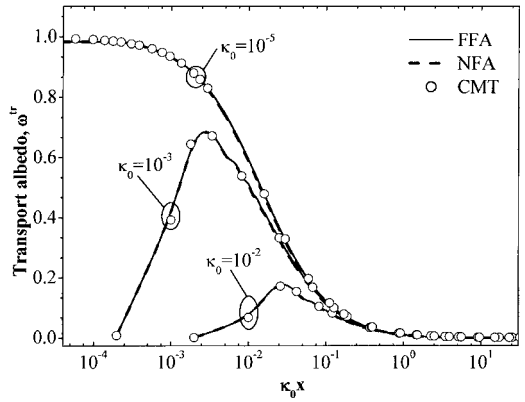

Fig. 11. Comparison among the CMT, NFA, and FFA transport albedos ω^{tr} for $n_0=1.4$ and $f_v=5\%$.

clusions can be valid for radiative properties of a bubble embedded in any arbitrary absorbing medium.

To complete this comparative study, the differences among the radiative transfer calculations using the FFA, NFA, and CMT should be assessed. Recall that in radiative transfer calculations the most important parameters are the transport extinction β^{tr} and single scattering albedo ω^{tr}, defined as[10,26]

$$\beta^{tr} = \alpha + \sigma(1-g), \tag{25}$$

$$\omega^{tr} = \frac{\sigma(1-g)}{\beta^{tr}}. \tag{26}$$

Thus the comparison of the transport coefficients β^{tr} and ω^{tr} permits one to compare the three approaches. Let us consider monodispersed bubbles randomly distributed in an absorbing and refracting matrix with $n_0=1.4$ and arbitrary values of κ_0, satisfying the independent scattering limit, e.g., $f_v=5\%$. The scattering phase function for the NFA is identical to that of the FFA, as assumed in the literature.[19,21] Figures 10 and 11 compare β^{tr} and ω^{tr} predicted by the three approaches as functions of the optical radius a_0. It is worth noting that even though important differences among these three approaches exist for the scattering efficiency factor and the asymmetry factor (Figs. 5–9), no significant difference is evident in the transport properties β^{tr} and ω^{tr} shown in Figs. 10 and 11. The differences in β^{tr} expected for large values of a_0 are masked by the absorption of the continuous phase (i.e., $\alpha_0 \approx \alpha$), since the bubble volume fraction is small in the independent scattering regime. Moreover, as a_0 increases, the albedo ω^{tr} becomes small and tends to 0 [$\sigma(1-g) \ll \beta^{tr}$]. As a result, the three approaches should yield identical results for transmittance and reflectance calculations in the independent scattering regime. This conclusion will be confirmed in Subsection 3.E by comparing the theoretical results based on the above models and experimental data for hemispherical transmittance and reflectance.

3. APPLICATION TO POROUS FUSED QUARTZ

A. Experimental Data of Volume Fraction and Bubble Size Distribution of Porous Fused Quartz

The above analysis shows that the bubble size distribution $n(a)$, the bubble volume fraction f_v, and/or the bubble average radius a_{32} are important for calculating the radiation characteristics.

The total volume fraction f_v can be evaluated by measuring the sample density[31]:

$$f_v = 1 - d_p/d_b, \tag{27}$$

where d_b and d_p refer to the dense and porous fused quartz densities, respectively. Several measurements of

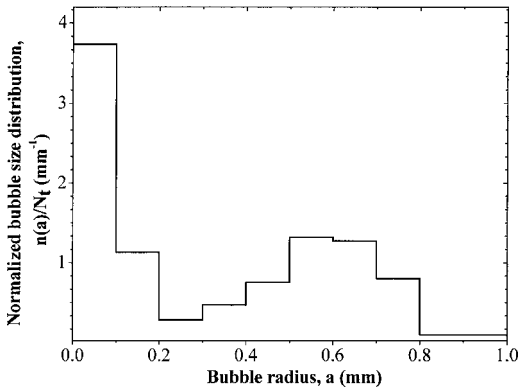

Fig. 12. Bubble normalized size distribution $n(a)/N_t$ for $N_t=212$ measured bubbles.

densities of dense and porous fused quartz samples give the bubble volume fraction equal to $f_v = 4.0\% \pm 0.5\%$.

The size distribution of bubbles for the thin sample was determined by analyzing high-resolution digital photographs.[31] From image analysis of the total number of bubbles $N_t = 212$, the bubble size distribution was determined and is depicted in Fig. 12. The corresponding bubble average radius is about $a_{32} = 0.64$ mm.

B. Infrared Optical Properties of Fused Quartz

The complex refraction index of fused quartz, $m_0 = n_0 + j\kappa_0$, is required in Eqs. (1) and (7)–(24). Different relations for the real part of the complex refraction index of fused quartz, n_0, as a function of wavelength have been suggested in the literature for different spectral regions.[32–35] The three-term Sellmeier equation proposed by Malitson[32] [Eq. (28) below] is the most commonly accepted expression in the literature for the spectral range from 0.21 to 6.7 μm at ambient temperature[22,31–33,36]:

$$n_0(\lambda) = \sqrt{1 + \frac{0.696\lambda^2}{\lambda^2 - 0.068^2} + \frac{0.407\lambda^2}{\lambda^2 - 0.114^2} + \frac{0.897\lambda^2}{\lambda^2 - 9.891^2}}. \tag{28}$$

The spectral value of κ_0 can be recovered from the normal spectral transmittance data denoted by $T(\lambda)$, based on the relationship between $T(\lambda)$ and κ_0 in which multiple internal reflections at the sample boundaries are accounted for[22,31,36]:

$$\kappa_0(\lambda) = -\frac{1}{4\pi e/\lambda} \times \ln\left\{ \frac{\sqrt{[1-\varepsilon(\lambda)]^4 + 4T(\lambda)^2[\varepsilon(\lambda)]^2} - [1-\varepsilon(\lambda)]^2}{2T(\lambda)[\varepsilon(\lambda)]^2} \right\}, \tag{29}$$

where e is the sample thickness and $\varepsilon(\lambda)$ is the spectral Fresnel reflectivity of the air–glass interface for normally incident radiation, given by[23,25]

$$\varepsilon(\lambda) = \frac{[1-n_0(\lambda)]^2 + [n_0(\lambda)]^2[\kappa_0(\lambda)]^2}{[1+n_0(\lambda)]^2 + [n_0(\lambda)]^2[\kappa_0(\lambda)]^2}. \tag{30}$$

In the case of dielectric materials, $\kappa_0^2 \ll 1$ and Eq. (30) simplifies to

$$\varepsilon(\lambda) = \frac{[1-n_0(\lambda)]^2}{[1+n_0(\lambda)]^2}. \tag{31}$$

The normal spectral transmittance of a 6.5 mm fused quartz sample thickness without bubbles and of identical composition to that of the porous fused quartz continuous phase was measured. The absorption index κ_0 was retrieved from Eq. (29). Figure 13 depicts the variation of the real refraction index n_0 predicted by Eq. (28), which is considered in this study, while Fig. 14 compares the values of κ_0 as a function of wavelength λ for the dense fused quartz with those reported in the literature.[34,35,37] The spectral value of the optical radius of a matrix particle, a_0, is also plotted in Fig. 14; the largest value of a_0 is found equal to 0.12 at 2.74 μm (with $x = 2\pi a_{32}/\lambda = 1467$) and 4 μm (with $x = 2\pi a_{32}/\lambda = 1000$).

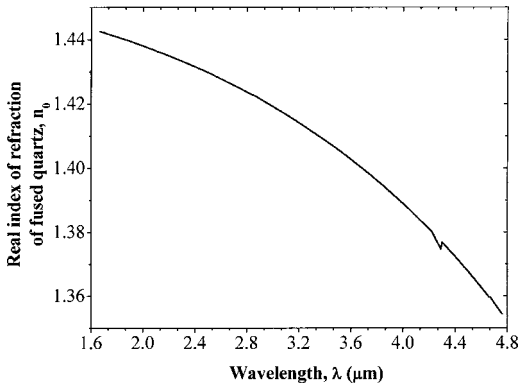

Fig. 13. Refraction index of fused quartz, n_0, calculated from Eq. (28).

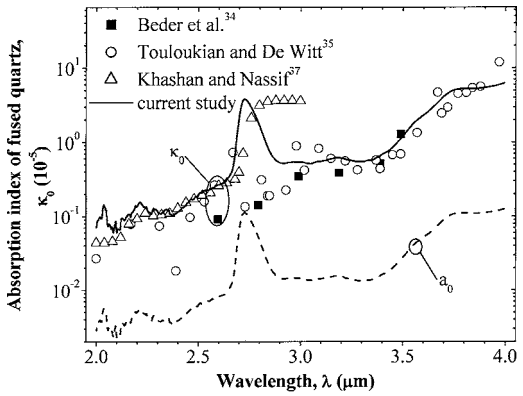

Fig. 14. Absorption index of fused quartz, κ_0, and the corresponding optical radius a_0, with $x = 2\pi a_{32}/\lambda$ and $a_{32} = 0.64$ mm.

C. Experimental Measurements of Radiation Characteristics

Experimental radiation characteristics of porous fused quartz such as the extinction coefficient $\beta_\lambda = \alpha_\lambda + \sigma_\lambda$, the scattering albedo $\omega_\lambda = \sigma_\lambda/\beta_\lambda$, and the scattering phase function asymmetry factor g are obtained by using an inverse method based on the minimization of the quadratic differences between measured and calculated spectral bidirectional transmittance and reflectance over discrete measurement directions. The measured bidirectional transmittance and reflectance are obtained from an experimental setup including a Fourier transform infrared (FTIR) spectrometer[22,36,38,39] operating in a spectral range from 1.67 to 14 μm, associated with a liquid-nitrogen-cooled mercury cadmium telluride detector mounted on a goniometric system.[36,39] The theoretical spectral bidirectional transmittance and reflectance are the solution of the radiative transfer equation (RTE) in a steady state regime, in the azimuthal symmetry case, and with the emission term disregarded thanks to the radiation modulation and the phase sensitive detection of the FTIR spectrometer. The radiation characteristics of three fused quartz samples of different thickness (5, 6, and 9.9 mm) were identified over more than 100 wavelengths

from 1.67 to 4.04 μm as reported by Randrianalisoa *et al.*[22] More details concerning this inverse method can be found in Refs. 22 and 36.

The experimental radiation characteristics used in this study are the averaged characteristics for three samples and are retrieved by using an inverse method. The experimental uncertainties associated with the radiation characteristics are assumed to be equal to the standard deviation of the radiation characteristics for the three sample thicknesses.

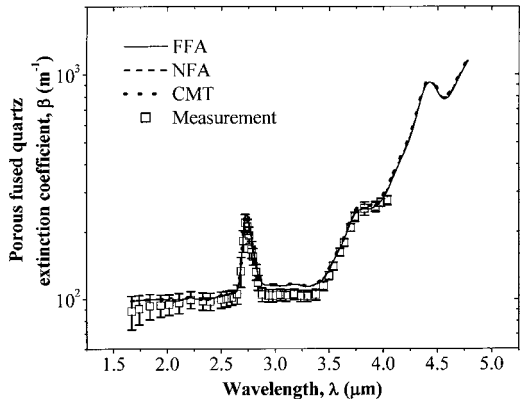

Fig. 15. Extinction coefficient β of porous fused quartz.

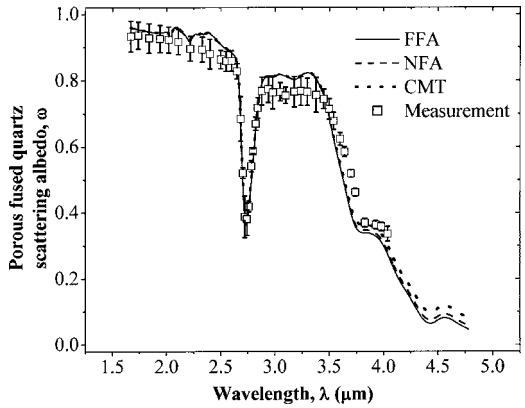

Fig. 16. Single scattering albedo ω of porous fused quartz.

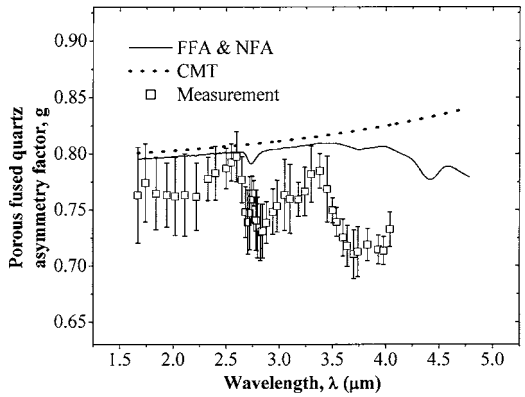

Fig. 17. Porous fused quartz asymmetry factor g. The asymmetry factors predicted by the FFA and NFA are identical.

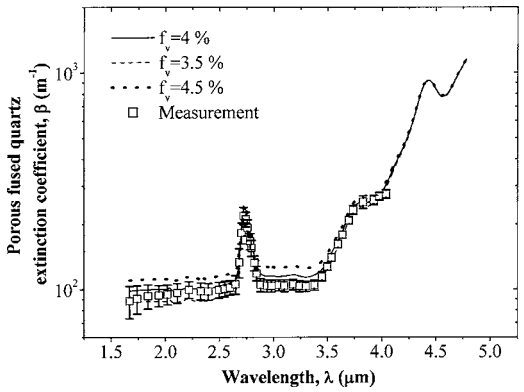

Fig. 18. Effect of the uncertainty in the porosity measurements on the predictions of the extinction coefficient β using the FFA.

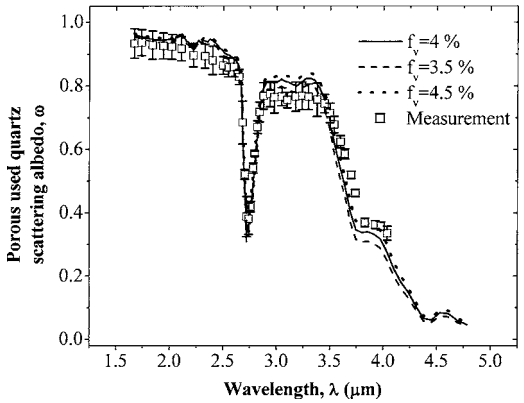

Fig. 19. Effect of the uncertainty in the porosity measurements on the predictions of the single scattering albedo ω using the FFA.

D. Comparison between Modeled and Measured Radiation Characteristics

The radiation characteristics predicted by the three models based on the FFA, NFA, and CMT are compared with those measured experimentally. The modeled radiation characteristics of the absorbing porous medium are obtained by introducing the bubble radiative properties (Q_s, Q_m, and ϕ), obtained from either the FFA, NFA, or CMT, in Eqs. (1), (2), and (5). Since bubbles embedded in the fused quartz are optically large (i.e., $x \gg 1$), the asymptotic solutions of the bubble efficiency factors and asymmetry factor [Eqs. (12)–(14)] are used for the CMT model. The extinction coefficient β, scattering albedo ω, and asymmetry factor g for porous fused quartz with an average porosity $f_v = 4\%$ are presented in Figs. 15–17. Figures 18 and 19 illustrate the effect of the experimental uncertainty of ±0.5% in the measured porosity on the radiation characteristics β and ω in the case of the FFA. The same order of magnitude uncertainties in β and ω are found for the FFA, NFA, and CMT. The largest uncertainty is equal to 23% for β and 17% for ω.

As is evident, there is good overall agreement among the three radiation characteristics models and the experimental results, except for the asymmetry factor for wavelengths larger than 3.5 μm. The deviation noted in the asymmetry factor can be attributed to (1) the uncertainties in the asymmetry factor g from the inverse method at

wavelengths larger than 3.5 μm, as discussed earlier,[22] and (2) the effect of the fused quartz absorption index κ_0 on g, which is not taken into account in the model based on the CMT.

E. Comparison between Theoretical and Experimental Hemispherical Transmittance and Reflectance

Comparison between the calculated and measured *hemispherical* transmittance and reflectance is also performed. The FTIR spectrometer is combined with a gold-coated integrating sphere (CSTM RSA-DI-40D) to measure the spectral hemispherical transmittance T^{+}_{exp} and reflectance T^{-}_{exp}. The associated experimental uncertainties are evaluated by repeating the measurements five times for each sample. These uncertainties vary with wavelength from 3% to 8% and 9% to 16% for the transmittance and the reflectance, respectively. To determine the hemispherical transmittance T^{+}_{th} and reflectance T^{-}_{th}, first, the

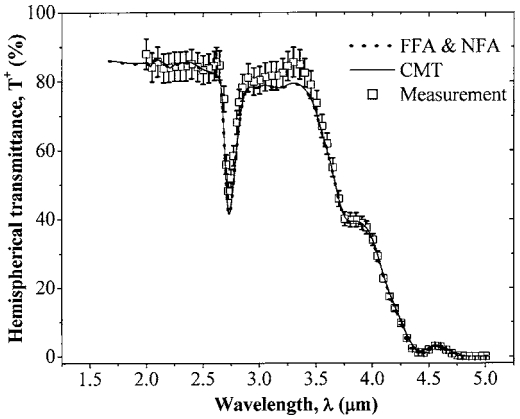

Fig. 20. Hemispherical transmittance T^{+} of the 5 mm thick sample. The results from the FFA and NFA are overlapping.

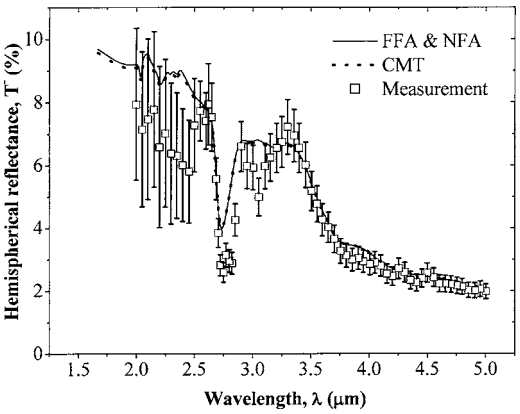

Fig. 21. Hemispherical reflectance T^{-} of the 5 mm thick sample. The results from the FFA and NFA are overlapping.

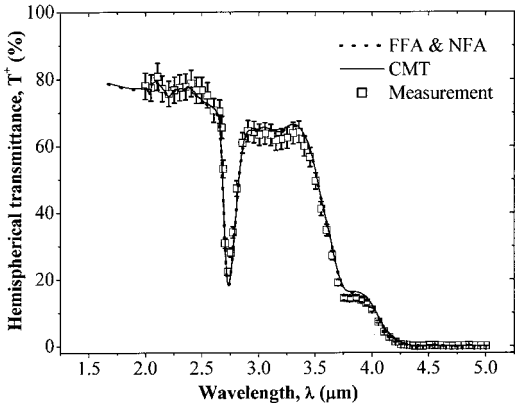

Fig. 22. Hemispherical transmittance T^{+} of the 9.9 mm thick sample. The results from the FFA and NFA are overlapping.

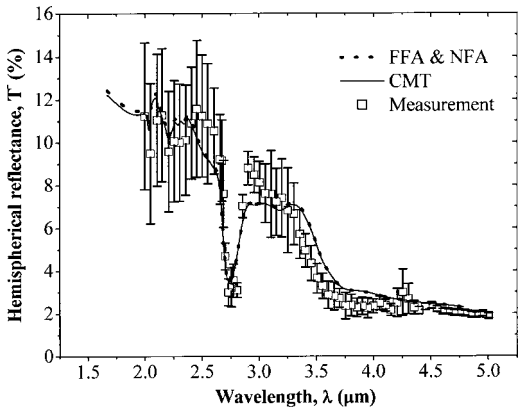

Fig. 23. Hemispherical reflectance T^{-} of the 9.9 mm thick sample. The results from the FFA and NFA are overlapping.

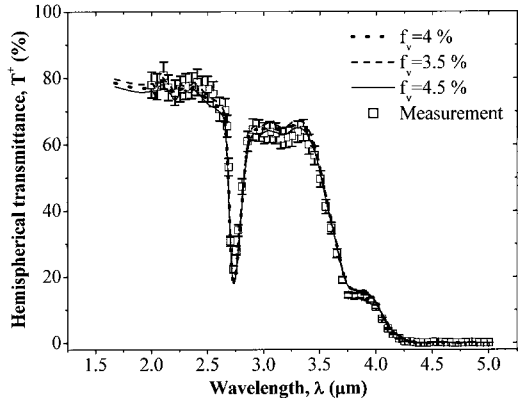

Fig. 24. Effect of the uncertainty in the porosity measurements on the predictions of the hemispherical transmittance T^{+} using the FFA for the 9.9 mm thick sample.

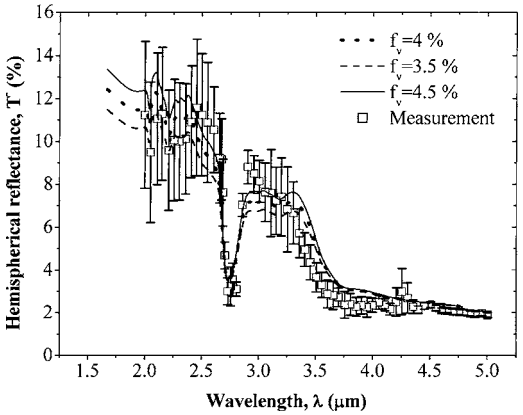

Fig. 25. Effect of the uncertainty in the porosity measurements on the predictions of the hemispherical reflectance T^{-} using the FFA for the 9.9 mm thick sample.

radiation characteristics β, ω, and Φ obtained from models using an average porosity of $f_v = 4\%$ are introduced in the RTE (Refs. 22 and 36) to compute the bidirectional transmittance and reflectance leaving the plane-parallel slab. Then, the hemispherical transmittance T_{th}^{+} and reflectance T_{th}^{-} are computed by integrating the bidirectional transmittance and reflectance over their respective hemispheres. Comparison between the calculated and measured hemispherical transmittance and reflectance are shown in Figs. 20–23 for the 5 mm and 9.9 mm thick samples. Very good agreement is observed between the transmittance and reflectance based on the FFA, NFA, and CMT radiation characteristics models and those measured experimentally. Moreover, the FFA and NFA results are overlapping. The differences observed in the asymmetry factor g (Fig. 17) between the FFA and the CMT are not evident in the hemispherical transmittance and reflectance results. This can be explained by the good agreement found for the transport parameters β^{tr} and ω^{tr}.

The effect of the uncertainty of the porosity measurement on the computed hemispherical transmittance T_{th}^{+} and reflectance T_{th}^{-} was found to be of the same order of magnitude as that of the measured hemispherical transmittance and reflectance uncertainties. They are 3.5% for the transmittance T_{th}^{+} and 15% for the reflectance T_{th}^{-}. The same uncertainties are observed for the results based on the FFA, NFA, and CMT radiation characteristics models. Figures 24 and 25 illustrate the effects of porosity uncertainties on the transmittance T_{th}^{+} and reflectance T_{th}^{-} based on the FFA.

Therefore one can conclude that the three abovementioned models for the radiation characteristics are valid for radiative transfer calculations of the hemispherical transmittances and reflectances of low porosity and weakly absorbing material.

4. CONCLUSIONS

Modeling of radiation characteristics of bubbles embedded in an absorbing medium has been presented. The models based on the classical Mie theory (CMT), the far field approximation (FFA), and the near field approximation (NFA) are compared with experimental data for the radiation characteristics as well as the hemispherical transmittance and reflectance of porous fused quartz. The following conclusions can be drawn:

- The bubble efficiency factors predicted by the FFA and NFA should be defined by using the true incident intensity on the particle instead of that at the particle center as in the conventional definition. This is required to avoid unphysical results when the bubbles are optically large and the matrix is highly absorbing.
- Large deviations are observed among the FFA, NFA, and CMT for the efficiency factors [scattering (Q_s) and absorption (Q_m)] and the asymmetry factor (g) of a bubble when the matrix is strongly absorbing and/or the bubble is optically large. However, all three approaches can be used to perform radiative transfer calculations in an absorbing matrix containing bubbles even if the matrix is strongly absorbing and the bubbles are optically large. Indeed, the disagreement observed among the three models is "masked" by the strong absorption of the matrix.
- Good agreement is observed between the experimental data and the predictions of the models for the radiation characteristics of porous fused quartz containing an ensemble of optically large polydispersed bubbles and having a porosity of 4%.
- The validity of the three radiation characteristics models in the independent scattering limit are confirmed by comparing the computed and measured hemispherical transmittances and reflectances of porous fused quartz samples of different thickness.

Corresponding author: Jaona Randrianalisoa, jaona.randrianalisoa@insa-lyon.fr.

REFERENCES

1. P. L. Marston, "Light scattering from bubbles in water," in *Procceedings of IEEE Oceans '89* (IEEE, 1989), pp. 1186–1193.
2. X. Zhang, M. Lewis, and B. Johnson, "Influence of bubbles on scattering of light in the ocean," Appl. Opt. **37**, 6525–6536 (1998).
3. A. G. Fedorov and L. Pilon, "Glass foam: formation, transport properties, and heat, mass, and radiation transfer," J. Non-Cryst. Solids **311**, 154–173 (2002).
4. A. Ungan and R. Viskanta, "Three-dimensional numerical modeling of circulation and heat transfer in a glass melting tank: Part 1. Mathematical formulation," Glastech. Ber. **60**, 71–78 (1987).
5. R. Viskanta and P. Mengüç, "Radiative transfer in dispersed media," Appl. Mech. Rev. **42**, 241–259 (1989).
6. D. Baillis and J. F. Sacadura, "Thermal radiation properties of dispersed media: theoretical prediction and experimental characterization," J. Quant. Spectrosc. Radiat. Transf. **67**, 327–363 (2000).
7. C. F. Bohren and D. R. Huffman, *Absorption and Scattering of Light by Small Particles* (Wiley, 1983).
8. A. G. Fedorov and R. Viskanta, "Radiation characteristics of glass foams," J. Am. Ceram. Soc. **83**, 2769–2776 (2000).
9. L. Pilon and R. Viskanta, "Apparent radiation characteristics of semitransparent media containing gas bubbles," in *Proceedings of the Twelfth International Heat Transfer Conference, France* (Elsevier, 2002), pp. 645–650.
10. L. A. Dombrovsky, "The propagation of infrared radiation in a semitransparent liquid containing gas bubbles," High Temp. **42**, 133–139 (2004).
11. W. C. Mundy, J. A. Roux, and A. M. Smith, "Mie scattering by spheres in an absorbing medium," J. Opt. Soc. Am. **64**, 1593–1597 (1974).
12. P. Chylek, "Light scattering by small particles in an absorbing medium," J. Opt. Soc. Am. **67**, 561–563 (1977).
13. P. Yang, B.-C. Gao, W. J. Wiscombe, M. I. Mishchenko, S. E. Platnick, H.-L. Huang, B. A. Baum, Y. X. Hu, D. M. Winker, S.-C. Tsay, and S. K. Park, "Inherent and apparent scattering properties of coated or uncoated spheres embedded in an absorbing host medium," Appl. Opt. **41**, 2740–2759 (2002).
14. I. W. Sudiarta and P. Chylek, "Mie-scattering formalism for spherical particle embedded in an absorbing medium," J. Opt. Soc. Am. A **18**, 1275–1278 (2001).
15. I. S. Sudiarta and P. Chylek, "Mie-scattering efficiency of a large spherical particle embedded in an absorbing medium," J. Quant. Spectrosc. Radiat. Transf. **70**, 709–714 (2001).
16. N. Lebedev, M. Gartz, U. Kreibig, and O. Stenzel, "Optical extinction by spherical particles in an absorbing medium: application to composite absorbing films," Eur. Phys. J. D **6**, 365–373 (1999).
17. N. Lebedev and O. Stenzel, "Optical extinction of an assembly of spherical particles in an absorbing medium:

application to silver clusters in absorbing organic materials," Eur. Phys. J. D **7**, 83–88 (1999).
18. Q. Fu and W. Sun, "Mie theory for light scattering by a spherical particle in an absorbing medium," Appl. Opt. **40**, 1354–1361 (2001).
19. W. Sun, G. N. Loeb, and Q. Fu, "Light scattering by coated sphere immersed in an absorbing medium: a comparison between the FDTD and analytic solutions," J. Quant. Spectrosc. Radiat. Transf. **83**, 483–492 (2004).
20. W. Sun, N. G. Loeb, and Q. Fu, "Finite-difference time domain solution of light scattering and absorption by particles in an absorbing medium," Appl. Opt. **41**, 5728–5743 (2002).
21. S. K. Sharma and A. R. Jones, "Absorption and scattering of electromagnetic radiation by a large absorbing sphere with highly absorbing spherical inclusions," J. Quant. Spectrosc. Radiat. Transf. **79-80**, 1051–1060 (2003).
22. J. Randrianalisoa, D. Baillis, and L. Pilon, "Improved inverse method for radiative characteristics of closed-cell absorbing porous media," J. Thermophys. Heat Transfer (to be published).
23. M. F. Modest, *Radiative Heat Transfer* (McGraw-Hill, 1993).
24. H. C. Hottel and A. F. Sarofim, *Radiative Transfer* (McGraw-Hill, 1967).
25. M. Q. Brewster, *Thermal Radiative Transfer and Properties* (Wiley, 1992).
26. L. A. Dombrovsky, *Radiation Heat Transfer in Disperse Systems* (Begell, 1996).
27. H. C. Van de Hulst, *Light Scattering by Small Particles* (Wiley, 1957).
28. M. Abramowitz, *Handbook of Mathematical Functions* (Dover, 1970).
29. R. Coquard and D. Baillis, "Radiative characteristics of opaque spherical particles beds: a new method of prediction," J. Thermophys. Heat Transfer **18**, 178–186 (2004).
30. B. P. Singh and M. Kaviany, "Independent theory versus direct simulation of radiative transfer in packed beds," Int. J. Heat Mass Transfer **34**, 2869–2882 (1991).
31. L. A. Dombrovsky, J. Randrianalisoa, and D. Baillis, "The use of Mie theory for analyzing experimental data to identify infrared properties of fused quartz containing bubbles," Appl. Opt. **44**, 7021–7031 (2005).
32. I. H. Malitson, "Interspecimen comparison of the refractive index of fused silica," J. Opt. Soc. Am. **55**, 1205–1209 (1965).
33. C. Z. Tan, "Determination of refractive index of silica glass for infrared wavelengths by IR spectroscopy," J. Non-Cryst. Solids **223**, 158–163 (1998).
34. E. C. Beder, C. D. Bass, and W. L. Shackleford, "Transmissivity and absorption of fused quartz between 0.2 μm and 3.5 μm from room temperature to 1500 degree C," Appl. Opt. **10**, 2263–2268 (1971).
35. Y. S. Touloukian and D. P. DeWitt, *Thermal Radiative Properties: Nonmetallic Solids*, Vol. 8 of Thermophysical Properties of Matter (Plenum, 1972).
36. D. Baillis, L. Pilon, H. Randrianalisoa, R. Gomez, and R. Viskanta, "Measurements of radiation characteristics of fused-quartz containing bubbles," J. Opt. Soc. Am. A **21**, 149–159 (2004).
37. M. A. Khashan and A. Y. Nassif, "Dispersion of the optical constants of quartz and polymethyl methacrylate glasses in a wide spectral range: 0.2–3 μm," Opt. Commun. **188**, 129–139 (2001).
38. D. Baillis and J. F. Sacadura, "Identification of polyurethane foam radiative properties—influence of transmittance measurements number," J. Thermophys. Heat Transfer **16**, 200–206 (2002).
39. V. P. Nicolau, M. Raynaud, and J. F. Sacadura, "Spectral radiative properties identification of fiber insulating materials," Int. J. Heat Mass Transfer **37**, 311–324 (1994).